3rd International Conference on Mechanical Models in Structural Engineering
CMMoST 2015
24-26 June 2015 Seville SPAIN

Modelling crack growth in quasi-brittle materials using mesh fragmentation technique

Maedo, Michael[1]; Manzoli, Osvaldo[2]; Bitencourt Jr., Luís[3]; Rodrigues, Eduardo[4]

ABSTRACT

The modelling of discontinuities with new finite element techniques (X-FEM and E-FEM) is cumbersome due to the need of algorithm tracking to simulate the crack growth. Therefore, a new technique to capture strong discontinuities in quasi-brittle materials without the need of a crack tracking scheme is presented. The method consists of inserting solid finite elements with high aspect ratio (ratio of the largest to the smallest dimension) between the bulk elements of the original mesh. Hence, when the ultimate tensile strength is reached only these interface elements are activated. Since the analyses are performed integrally in the context of the continuum mechanics, there is no need to use tracking algorithms to simulate the formation of cracks. The study is performed using different specimens in order to cover the cases that can show up in practice. Numerical results show that the technique is able to represent crack growth.

Keywords: solid finite elements with high aspect ratio, tensile damage model, quasi-brittle materials, crack growth, strong discontinuities.

1. INTRODUCTION

The formation and propagation of cracks involves many engineering fields. In concrete, the crack process rules the nonlinear behaviour of the material, so that significant cracks can lead the material to a structural collapse. On the other hand, in soil mechanics the formation and propagation of cracks may affect the soil, decreasing its strength and sometimes causing erosions.

In recent years, there are many techniques to represent crack growth in quasi-brittle materials. In the context of the finite element method, some methods such as E-FEM[1,2,3] and X-FEM[4,5] require tracking algorithms to represent crack growth. These tracking techniques are simple to represent a few cracks in 2D analyses, but are very complex for 3D problems.

Thus, in order to describe the crack process without the need of crack tracking schemes, a new technique that consists of introducing in special interface elements between the regular elements of the mesh is proposed [6,7]. Thereby, these special elements must be able to represent the discontinuities, and consequently, the cracks develop along the boundaries of the regular elements.

[1] *Department of Mechanical Engineering. UNESP – Sao Paulo State University (BRAZIL). michaelmaedo@yahoo.com.br (Corresponding author)*
[2] *Department of Civil Engineering. UNESP – Sao Paulo State University (BRAZIL). omanzoli@feb.unesp.br*
[3] *Polytechnic School. USP – University of Sao Paulo (BRAZIL). luis.bitencourt@usp.br*
[4] *Polytechnic School. USP – University of Sao Paulo (BRAZIL). eduardoalex@usp.br*

However, instead of zero-thickness interface elements this work presents a new technique that uses solid finite elements with high aspect ratio (ratio of the larges to the smallest dimension) to represent discontinuities. Throughout this paper it is shown that, as the aspect ratio increases, the element strain also increase, approaching the kinematics associated to the discontinuity, as in the case of Continuum Strong Discontinuity Approach (CSDA) [8,9]. Thus, based on the same principles of the CSDA, bounded stresses are obtained from unbounded strains.

To model the nonlinear behaviour of the interfaces, a tensile damage constitutive model that relates stress to strain is described. Since the analyses are performed integrally in the context of the continuum mechanics, complex crack patterns and 3D cracks can be properly addressed using the technique proposed.

2. INTERFACE SOLID FINITE ELEMENT

Let us consider a three-node triangular finite element, with base b given by the distance between nodes 2 and 3, and height h formed by the segment between node 1 and its projection on the base of the element, as shown in Fig. 1.

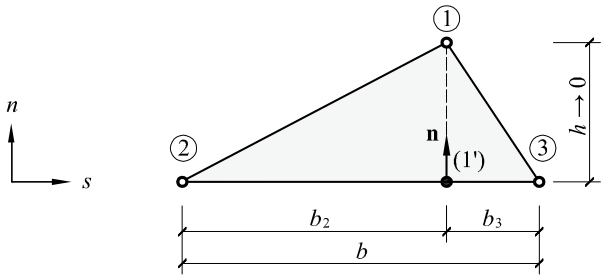

Figure 1. *Interface triangular element in the coordinate system* (s,n)[10]

Assuming the coordinate system (s,n), where $\mathbf{n}$ is the unit normal to the base of the element, the strain tensor for any point can be written as follows [10]:

$$\boldsymbol{\varepsilon} = \tilde{\boldsymbol{\varepsilon}} + \hat{\boldsymbol{\varepsilon}} \tag{1}$$

with

$$\tilde{\boldsymbol{\varepsilon}} = \frac{1}{b}\begin{bmatrix} 0 & \frac{1}{2}\left(u_n^{(3)} - u_n^{(2)}\right) & 0 \\ \frac{1}{2}\left(u_n^{(3)} - u_n^{(2)}\right) & \left(u_s^{(3)} - u_s^{(2)}\right) & 0 \\ 0 & 0 & 0 \end{bmatrix} \tag{2}$$

and

$$\hat{\boldsymbol{\varepsilon}} = \frac{1}{h}\begin{bmatrix} [\![u]\!]_n & \frac{1}{2}[\![u]\!]_s & 0 \\ \frac{1}{2}[\![u]\!]_s & 0 & 0 \\ 0 & 0 & 0 \end{bmatrix} \tag{3}$$

where $u_n^{(i)}$ and $u_s^{(i)}$ are the components of the displacement of node i in the n and s directions, respectively; and $[\![u]\!]_n = u_n^1 - u_n^{1'}$ and $[\![u]\!]_s = u_s^1 - u_s^{1'}$ are the components of the relative displacement between node 1 and its projection on the base (1').

The part of the strain tensor that depends on the height h, which is expressed b Eq. (3), can be written in a more general form as:

$$\hat{\boldsymbol{\varepsilon}} = \frac{1}{h}(\mathbf{n} \otimes [\![\mathbf{u}]\!])^S \tag{4}$$

where $(\cdot)^S$ is the symmetric part of $(\cdot)$, $[\![\mathbf{u}]\!]$ is relative displacement between node 1 and the projection (1') and $\otimes$ is the dyadic product. Thus, substituting Eq. (4) into (1), we obtain:

$$\boldsymbol{\varepsilon} = \underbrace{\tilde{\boldsymbol{\varepsilon}}}_{\text{bounded}} + \underbrace{\frac{1}{h}(\mathbf{n} \otimes [\![\mathbf{u}]\!])^S}_{\text{unbounded}} \tag{5}$$

Taking the limit as $h \to 0$, the strain component $\tilde{\boldsymbol{\varepsilon}}$ remains bounded while $\hat{\boldsymbol{\varepsilon}}$ becomes unbounded. In this case, the deformations of the element are almost exclusively defined by the displacements between node 1 and its projection on the base of the element. Note that, when h tends to zero, node 1 and the projection (1') converge to the same material point. Therefore, $[\![\mathbf{u}]\!]$ becomes the measure of the strong discontinuity.

The strain field given by Eq. (5) consists of the kinematics of the CSDA, and consequently, the same applications of the CSDA can be treated with finite elements with high aspect ratio [6].

3. TENSILE DAMAGE MODEL

The tensile damage model is designed to describe crack growth in quasi-brittle materials. The damage criterion is based on the component of the tensile stress normal to the base of the element with high aspect ratio, so that the model is able to represent the crack process in mode I. It is worth mentioning that this model degrades all components of the effective stress, and therefore the crack initiation can evolve in mixed mode.

3.1. Continuum constitutive model

The continuum damage model proposed is defined by the following constitutive relation:

$$\boldsymbol{\sigma} = (1 - d)\overline{\boldsymbol{\sigma}} \tag{6}$$

where $\boldsymbol{\sigma}$ is the stress tensor, $d \in [0,1]$ is the damage variable, and $\overline{\boldsymbol{\sigma}}$ is the effective stress tensor expressed as:

$$\overline{\boldsymbol{\sigma}} = \mathbf{C} : \boldsymbol{\varepsilon} \tag{7}$$

where $\mathbf{C} = 2G\mathbf{I} + (K + 2/3G)\mathbf{1} \otimes \mathbf{1}$ is the fourth order elastic tensor, G is the shear modulus, K is the bulk modulus, $\mathbf{I}$ is the fourth order unit tensor, and $\mathbf{1}$ is the second order unit tensor.

The damage criterion is based on the component of the stress normal to the base of the element, in other words:

$$\phi = \sigma_{nn} - q(r) \leq 0 \tag{8}$$

Where q and r are the stress and strain-like internal variables, respectively

Dividing Eq. (8) by $(1-d)$, the damage criterion can be rewritten as:

$$\bar{\phi} = \bar{\sigma}_{nn} - r \leq 0 \tag{9}$$

Since $r = q/(1-d)$, the damage evolution rule is given by

$$d(r) = 1 - \frac{q(r)}{r} \tag{10}$$

The constitutive model is completed by the Kuhn-Tucker relations

$$\bar{\phi} \leq 0;\ \dot{r} \geq 0; \dot{r}\,\bar{\phi} = 0 \tag{11}$$

and the consistency condition

$$\dot{r}\,\dot{\bar{\phi}} = 0 \text{ if } \bar{\phi} = 0 \tag{12}$$

Based on Eqs. (9), (11), and (12), the evolution law for the strain-like internal variable can be expressed as:

$$r(t) = \max_{S\in[0,t]}[\bar{\tau}(s), f_t] \tag{13}$$

Thus, r assumes the maximum value that $\bar{\sigma}_{nn}$ reaches throughout the loading process, starting from the initial tensile strength of the material f_t.

3.2. Discrete constitutive relation

In the limit case of strong discontinuity, the continuum constitutive relation given by Eq. (6) becomes a discrete constitutive relation that relates the interface stresses to the components of the displacement jump. Therefore,

$$\begin{aligned}\mathbf{t} &= \lim_{h\to 0} \boldsymbol{\sigma}\cdot\mathbf{n} = \lim_{h\to 0}(1-d)\mathbf{n}\cdot\mathbf{C} : (\tilde{\boldsymbol{\varepsilon}} + \hat{\boldsymbol{\varepsilon}}) = \lim_{h\to 0}(1-d)\mathbf{n}\cdot\mathbf{C} : \left(\tilde{\boldsymbol{\varepsilon}} + \frac{1}{h}(\mathbf{n}\otimes[\![\mathbf{u}]\!])^S\right) \\ &= \lim_{h\to 0}\frac{(1-d)}{h}\,\mathbf{n}\cdot\mathbf{C} : [h\,\tilde{\boldsymbol{\varepsilon}} + (\mathbf{n}\otimes[\![\mathbf{u}]\!])^S] \\ &= \lim_{h\to 0}\underbrace{\left[\frac{(1-d)}{h}\,(\mathbf{n}\cdot\mathbf{C}\cdot\mathbf{n})\right]}_{\widehat{\mathbf{K}}}\cdot[\![\mathbf{u}]\!] = \lim_{h\to 0}\widehat{\mathbf{K}}\cdot[\![\mathbf{u}]\!]\end{aligned} \tag{14}$$

where $\mathbf{t} = \{\sigma_{nn}\ \sigma_{ns}\ \sigma_{nt}\}^{\mathrm{T}}$, $[\![\mathbf{u}]\!] = \{[\![u]\!]_n\ \ [\![u]\!]_s\ \ [\![u]\!]_t\}^{\mathrm{T}}$ and

$$\widehat{\boldsymbol{K}} = \frac{(1-d)}{h}\begin{bmatrix} 4/3G + K & 0 & 0 \\ 0 & G & 0 \\ 0 & 0 & G \end{bmatrix} \tag{15}$$

According to CSDA, the stresses remain bounded even for unbounded strains. In the case of the element with high aspect ratio, to maintain the stresses bounded when $h \to 0$, the components of the displacement jump must tend to zero in the elastic regime $(d = 0)$. On the other hand, in the inelastic regime $([\![\mathbf{u}]\!] \neq 0)$, the damage variable d must tends to 1 to hold the stresses bounded.

Assuming Poisson's ratio null $(\nu = 0)$, we obtain:

$$4G/3 + K = E \text{ and } G = E/2 \tag{16}$$

and therefore, the discrete relation can be written in terms of the Young's modulus.

Table 1 shows the continuum and discrete constitutive expressions for the tensile damage model.

Table 1. Continuum and discrete tensile damage models

	Continuum model	**Discrete model**
Constitutive relation	$\boldsymbol{\sigma} = (1-d)\bar{\boldsymbol{\sigma}}$ $\bar{\boldsymbol{\sigma}} = \mathbf{C}\colon\boldsymbol{\varepsilon}$	$\mathbf{t} = \widehat{\mathbf{K}} \cdot [\![\boldsymbol{u}]\!]$
Equivalent stress	$\bar{\tau} = \bar{\sigma}_{nn}$	$\bar{\tau} = \bar{\sigma}_{nn} = \frac{1}{h} E [\![u]\!]_n$
Damage criterion	$\bar{\phi} = \bar{\tau} - r \leq 0$	$\bar{\phi} = \bar{\tau} - r \leq 0$
Evolution law for the strain-type variable	$r = \max_{s\in[0,t]} [\bar{\tau}(s), f_t]$	$r = \max_{s\in[0,t]} [\bar{\tau}(s), f_t]$
Damage evolution	$d(r) = 1 - \frac{q(r)}{r}$	$d(r) = 1 - \frac{q(r)}{r}$
Hardening law	$q(r)$	$q(r)$

The evolution of the normal stress for a normal displacement monotonically increasing in mode I (i.e. $[\![\dot{u}]\!]_n \geq 0, [\![u]\!]_n \big|_{t=0} = 0, [\![u]\!]_s = [\![u]\!]_t = 0$) is:

$$\sigma_{nn}([\![u]\!]_n) = \frac{(1-d)}{h} E [\![u]\!]_n = \begin{cases} {}^{1}\!/_{h}\, E [\![u]\!]_n & \text{if } [\![u]\!] \leq [\![u_0]\!]_n \\ q\left({}^{1}\!/_{h}\, E [\![u]\!]_n\right) & \text{if } [\![u]\!] > [\![u_0]\!]_n \end{cases} \tag{17}$$

with $[\![u_0]\!]_n = h\, f_t/E$.

Let us assume that the hardening law is governed by the following exponential equation:

$$q(r) = f_t e^{A\, h(1 - r/f_t)} \tag{18}$$

where f_t is the tensile strength of the material and A is the softening parameter. Thus, the energy dissipated in a complete degradation process in mode one of the interface element is

$$G_f = \int_0^{\infty} \sigma_{nn}(\llbracket u \rrbracket_n)\, \mathrm{d}\llbracket u \rrbracket_n = \int_0^{\llbracket u_0 \rrbracket_n} \sigma_{nn}(\llbracket u \rrbracket_n)\, \mathrm{d}\llbracket u \rrbracket_n + \int_{\llbracket u_0 \rrbracket_n}^{\infty} \sigma_{nn}(\llbracket u \rrbracket_n)\, \mathrm{d}\llbracket u \rrbracket_n$$
$$= \int_0^{\llbracket u_0 \rrbracket_n} {}^{1}\!/_{h}\, E \llbracket u \rrbracket_n\, \mathrm{d}\llbracket u \rrbracket_n + \int_{\llbracket u_0 \rrbracket_n}^{\infty} q\left({}^{1}\!/_{h}\, E \llbracket u \rrbracket_n\right) \mathrm{d}\llbracket u \rrbracket_n = \frac{(f_t^2 h/2 + f_t^2/A)}{E} \tag{19}$$

Taking the limit as $h \to 0$, the fracture energy becomes:

$$G_f = \frac{f_t^2}{A\, E} \tag{20}$$

From Eq. (20), we can define the softening parameter in terms of the material properties, i.e.

$$A = \frac{f_t^2}{G_f\, E} \tag{21}$$

4. NUMERICAL EXAMPLES

The 2D numerical analyses were performed using three-node triangular finite element, while in 3D cases, tetrahedron finite elements were used in simulations. To describe crack growth, interfaces elements are inserted between the bulk (regular) elements of the mesh. Although in some cases the entire mesh is fragmented, in general only the part of the mesh corresponding to the region of study is fragmented, reducing computational effort and consequently time process.

As previously mentioned, the interfaces are represented using elements with high aspect ratio, which are modelled using the tensile damage model equipped with exponential softening.

4.1. Gravity dam

In order to show the capability of the technique to predict cracks in quasi-brittle materials, the gravity dam, tested experimentally by Carpinteri et al. [11], is analysed by assuming the geometry and boundary conditions shown in Fig. 2. The thickness of the specimen is 300 mm and the depth of the notch of the dam is 150 mm.

For the numerical analyses, the behaviour of the bulk elements is governed by the linear elastic model with $E = 35.7$ GPa, and $\nu = 0.1$. On the other hand, for the elements with high aspect ratio the following material properties are assumed: $E = 35.7$ GPa, $\nu = 0$, $G_f = 184$ N/m, and $f_t = 3.6$ MPa.

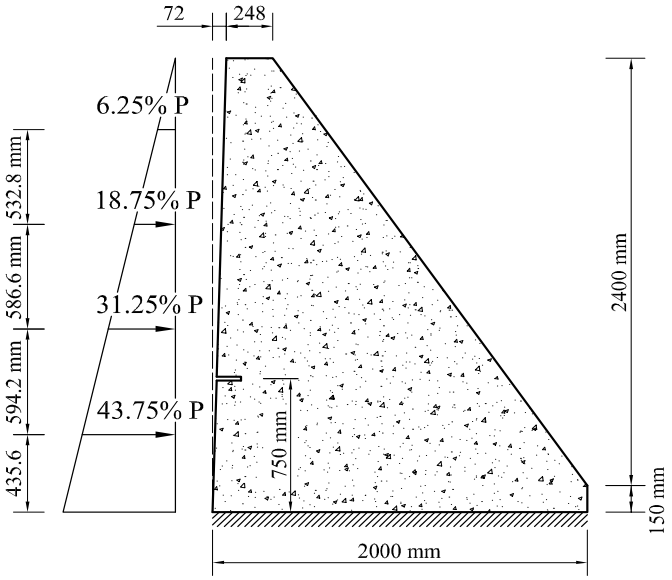

Figure 2. *Gravity dam: geometry and boundary conditions.*

The analyses were performed using three unstructured meshes with different refinements. Fig. 3 shows the crack pattern at the end of the analysis for all meshes studied. As can be seen from Fig. 4a, the structural responses, in terms of the load vs. CMOD (Crack Mouth Opening Displacement), derived from the numerical results are compared with the experimental one. Moreover, the numerical and experimental crack trajectories were contrasted as illustrated in Fig. 4b.

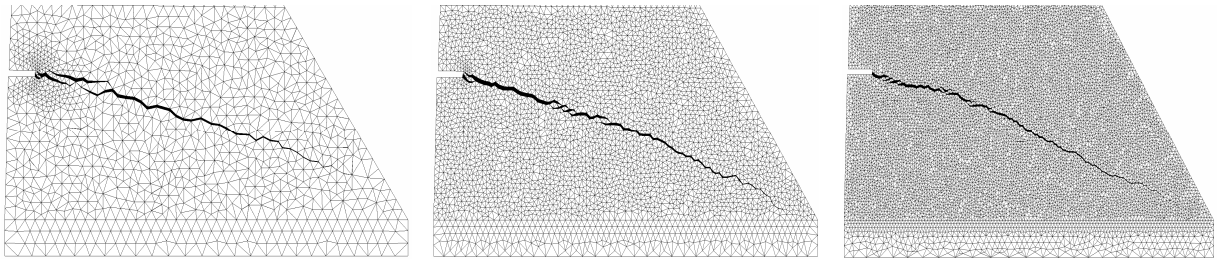

Figure 3. *Gravity dam: deformed meshes.*

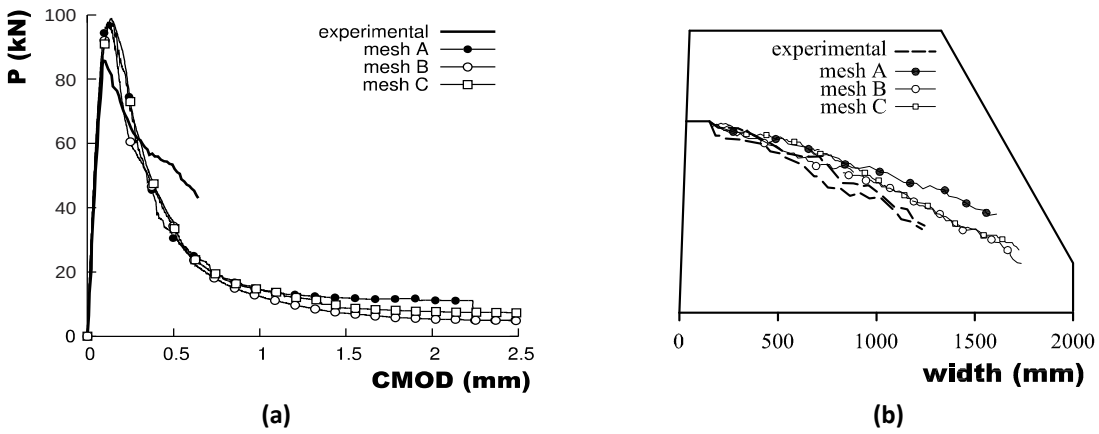

Figure 4. *Gravity dam: (a) structural responses; (b) crack paths.*

4.2. Four point bending test

In order to study the technique with respect to the mesh dependency, the notched beam tested by Arrea and Ingraffea [12] is simulated. The geometry and the boundary conditions of the problem are sketched in Fig. 5, where the thickness is 150 mm.

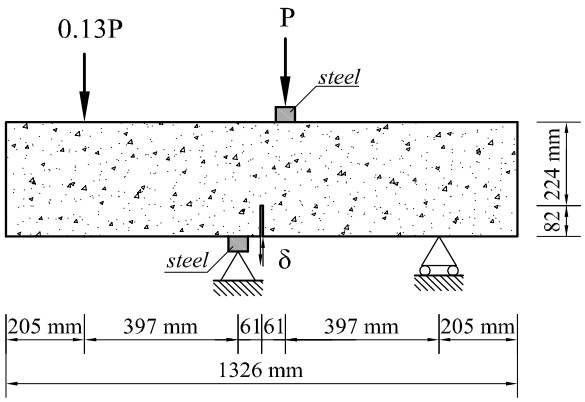

Figure 5. *Four point bending test: geometry and boundary conditions.*

The considered material properties of the bulk elements are $E = 28.8\ \text{GPa}$ and $\nu = 0.18$. For the interface elements, the following material parameters have been adopted: $E = 28.8\ \text{GPa}$, $\nu = 0$, $G_f = 100\ \text{N/m}$, and $f_t = 2.8\ \text{MPa}$.

Six meshes, three unstructured and three structured, were used to study mesh dependency. Fig. 6 shows the crack trajectory for the six meshes, where the A, B and C meshes are the unstructured ones, and the A', B' and C' meshes are structured.

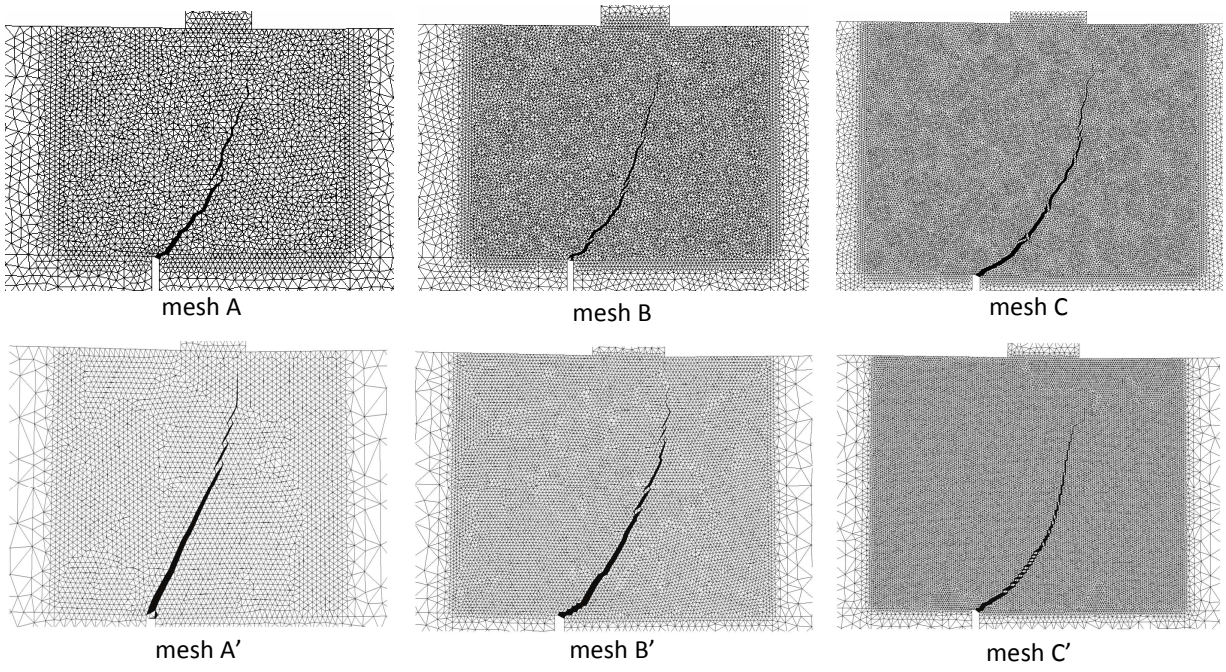

Figure 6. *Four point bending test: deformed meshes.*

Fig. 7a-c illustrates the numerical and experimental results in terms of load vs. δ (which is the crack mouth sliding displacement). Thus, in Fig. 7a the curves of the unstructured meshes are shown to fit very well in the experimental region. On the other hand, the structural response of the structured meshes deviates from the experimental band in some cases. Fig 7c compares all obtained results. Fig. 7d-f presents the load-deflection at the point where P is applied. Thereby, Fig. 7d and 7e show the load-deflection curve of the unstructured and structured meshes, respectively. Analogously to Fig. 7c, the response of the six meshes is shown in Fig. 7f.

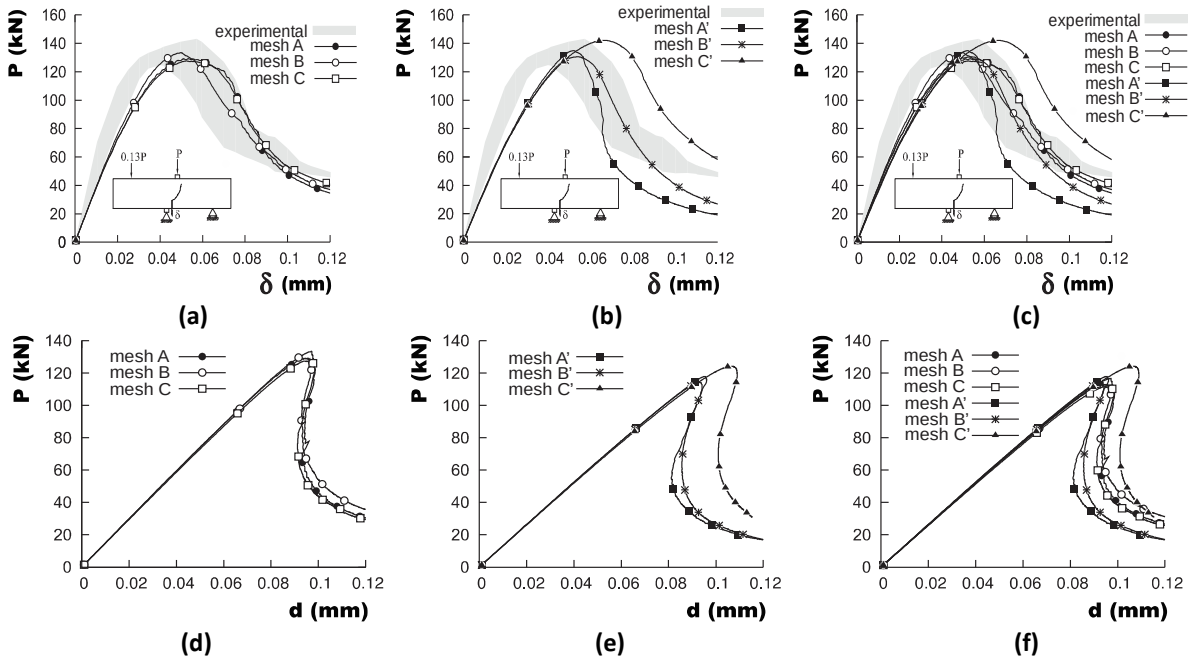

Figure 7. *Four point bending test: (a) load vs. CMSD curves of the unstructured meshes; (b) load vs. CMSD curves of the structured meshes; (c) load vs. CMSD curves of the unstructured and structured meshes; (d) load-deflection curves of the unstructured meshes; (e) load-deflection curves of the structured meshes; (f) load-deflection curves of the unstructured and structured meshes.*

4.3. Three point bending test

This test is performed to show that the technique is also able to predict crack growth by assuming a three-dimensional analysis. Hence, the three point bending test reported by Béllego et al. [13] was studied by considering both 2D and 3D analyses. The dimensions and the boundary conditions of the problem are indicated in Fig. 8 and the thickness of the specimen is 40 mm.

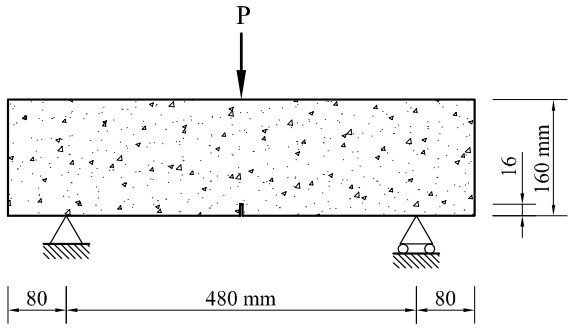

Figure 8. *Three point bending test: geometry and boundary conditions.*

The material parameters of the bulk elements are $E = 38.5\ \text{GPa}$ and $\nu = 0.24$. In the case of the interface elements, we assume $E = 38.5\ \text{GPa}$, $\nu = 0.24$, $G_f = 50\ \text{N/m}$, and $f_t = 3.6\ \text{MPa}$.

The analyses were performed using three different 2D unstructured meshes and three different 3D meshes. The crack paths for 2D and 3D analyses are shown in Figs. 9 and 10, respectively.

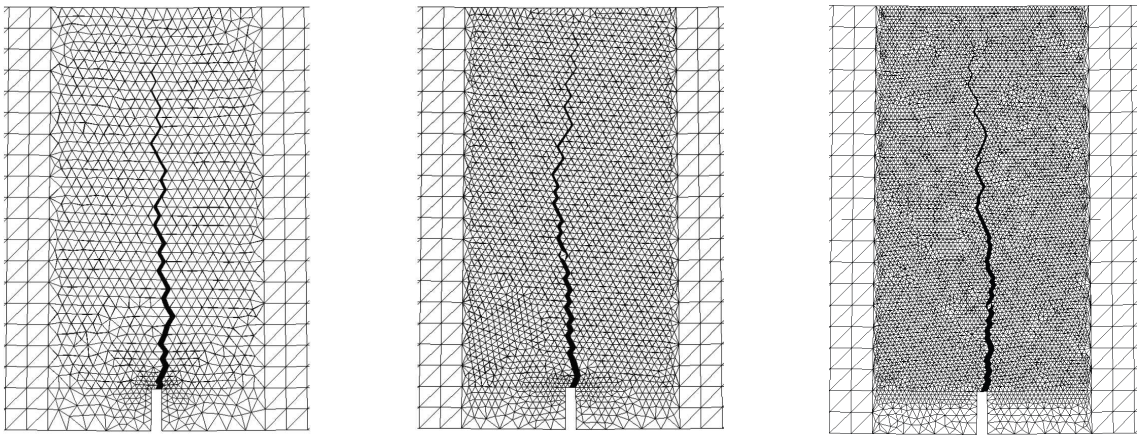

Figure 9. *Three point bending test: 2D deformed meshes.*

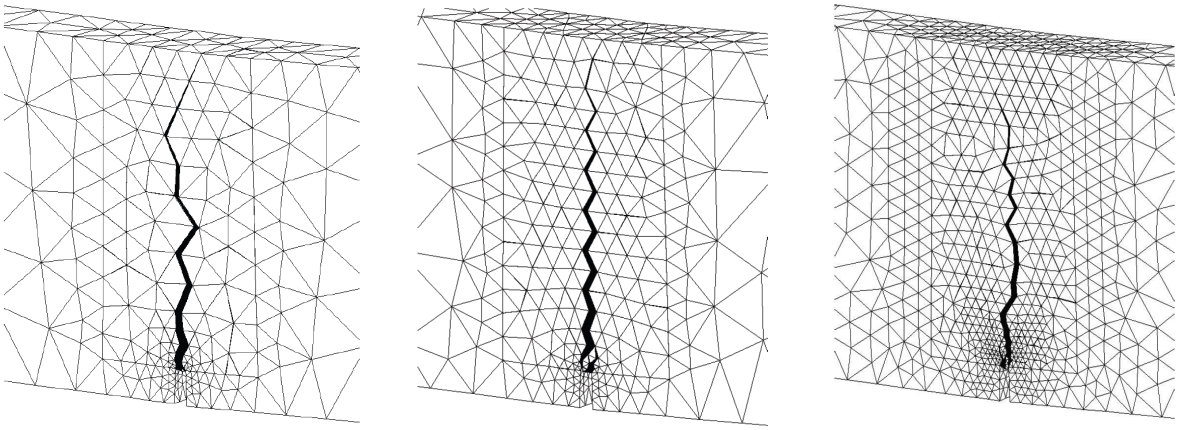

Figure 10. *Three point bending test: 3D deformed meshes.*

Figs. 11a and 11b show the obtained results, in terms of the load vs. displacement at the point where the load is applied, for 2D and 3D analyses respectively. Finally, Fig. 11c contrasts 2D and 3D structural responses.

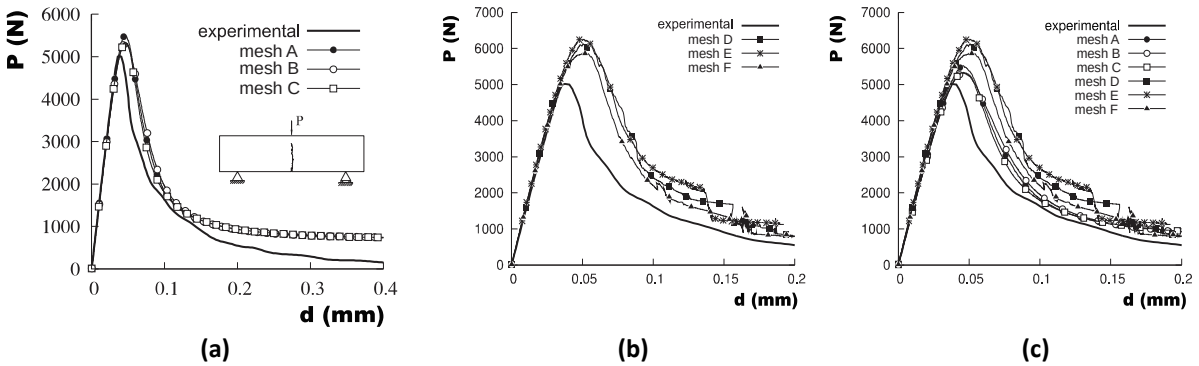

Figure 11. *Three point bending test: (a) structural responses for 2D analyses; (b) structural responses for 3D analyses; (c) structural responses for 2D and 3D analyses.*

5. CONCLUDING REMARKS

Triangular finite elements in 2D and tetrahedron finite elements in 3D are able to describe the kinematics of strong discontinuities. Thereby, these elements can be employed to simulate crack growth in the context of the CSDA.

The tensile damage model based on the component of the tensile stresses normal to the base of these interface elements is able to depict the crack process in quasi-brittle materials. In the limit situation of strong discontinuity the continuum damage model tends to a discrete (cohesive) damage model, so that the softening law is related to the fracture energy.

The mesh fragmentation technique, which consists of inserting elements with high aspect ratio between the regular elements of the mesh, shown be properly to represent crack growth in quasi-brittle materials. As mentioned before, since the analysis is performed integrally in the context of the continuum mechanics, there is no need of tracking algorithms during the analysis. As a consequence, 3D analysis can be properly addressed with the proposed technique.

Although the technique seems to be dependent of the mesh, no significant mesh dependency is observed when it is used unstructured meshes. The zigzag crack path caused by the technique affects neither the structural responses nor the crack pattern predictions.

ACKNOWLEDGEMENTS

The authors would like to thank the financial support provided by FAPESP (Sao Paulo Research Foundation), as well as CNPQ (National Council for Scientific and Technological Development) and CAPES (Coordination for Improvement of Higher Education Personnel).

REFERENCES

[1] Oliver, J., Huespe, A. E., Pulido, M. D. G., & Chaves, E. (2002). From continuum mechanics to fracture mechanics: the strong discontinuity approach.*Engineering Fracture Mechanics*, *69*(2), 113-136.

[2] Oliver, J., Huespe, A. E., & Samaniego, E. (2003). A study on finite elements for capturing strong discontinuities. *International journal for numerical methods in engineering*, *56*(14), 2135-2161.

[3] Oliver, J., Huespe, A. E., Samaniego, E., & Chaves, E. W. V. (2004). Continuum approach to the numerical simulation of material failure in concrete.*International Journal for Numerical and Analytical Methods in Geomechanics*, *28*(7-8), 609-632.

[4] Belytschko, T., & Black, T. (1999). Elastic crack growth in finite elements with minimal remeshing. *International journal for numerical methods in engineering*, *45*(5), 601-620.

[5] Belytschko, T., Gracie, R., & Ventura, G. (2009). A review of extended/generalized finite element methods for material modeling. *Modelling and Simulation in Materials Science and Engineering*, *17*(4), 043001.

[6] Manzoli, O. L., Maedo, M. A., Rodrigues, E. A., & Bittencourt, T. N. (2014). Modeling of multiple cracks in reinforced concrete members using solid finite elements with high aspect ratio. *Bicanic et al., editors. Computational modeling of concrete structures*, *1*, 383-92.

[7] Sánchez, M., Manzoli, O. L., & Guimarães, L. J. (2014). Modeling 3-D desiccation soil crack networks using a mesh fragmentation technique. *Computers and Geotechnics*, *62*, 27-39.

[8] Oliver, J., Cervera, M., & Manzoli, O. (1999). Strong discontinuities and continuum plasticity models: the strong discontinuity approach. *International journal of plasticity*, *15*(3), 319-351.

[9] Oliver, J. (1996). Modelling strong discontinuities in solid mechanics via strain softening constitutive equations. Part 1: Fundamentals. *International journal for numerical methods in engineering*, *39*(21), 3575-3600.

[10] Manzoli, O. L., Gamino, A. L., Rodrigues, E. A., & Claro, G. K. S. (2012). Modeling of interfaces in two-dimensional problems using solid finite elements with high aspect ratio. *Computers & Structures*, *94*, 70-82.

[11] Carpinteri, A., Cornetti, P., Barpi, F., & Valente, S. (2003). Cohesive crack model description of ductile to brittle size-scale transition: dimensional analysis vs. renormalization group theory. *Engineering fracture mechanics*, *70*(14), 1809-1839.

[12] Arrea, M., Ingraffea, A.R. (1982). Mixed-mode crack propagation in mortar and concrete (Technical Report 81-13). New York: Cornell University.

[13] Le Bellégo, C., Dubé, J. F., Pijaudier-Cabot, G., & Gérard, B. (2003). Calibration of nonlocal damage model from size effect tests. *European Journal of Mechanics-A/Solids*, *22*(1), 33-46.